CHAPTER 3

GREEN SYNTHESIS AND CHARACTERIZATION OF Ag, Au AND Cu NANOPARTICLES

Syntheses and characterizations of Ag, Au and Cu NPs in presence of rich starch as stabilizer is presented in this as separate sections. Results and discussion of each of them are included in respective sections. Stabilities of sols have been compared and a possible mechanism is also discussed. Conclusions drawn from this part of the investigations are given at the end.

3.1 Introduction

Several green methods have been utilized as alternative approaches for the synthesis of NPs, which are environmental friendly, non-toxic or nonhazardous, cheap, and simple [152]. In particular, the synthesis of metallic NPs using constituents of bio-friendly ingredients has received attention during the last decade. This has happened not only due to novel physical and chemical properties inherent to metallic NPs [153] and potential applications in the areas of optics [154–157], electronics [153], catalysis [158, 159] etc., but also as environmental friendly approach adaptable for biological and medicinal applications [22–24, 160]. A precise control of the shape and size of these NPs is essential for the applications in many of the areas. The NPs needed to be compatible with biological systems in addition to the requirements of microstructural control for biomedical applications. The work reported on biosynthesis of gold (Au) NPs employing alfalfa by

Gardea-Torresdey et al. in 2002 [161], has opened up the area of biosynthesis of metallic NPs using different parts of plants such as leaves exploiting the reduction and stabilization potentials of their constituents such as proteins, polysaccharides, and vitamins [162–166]. For example, biosynthesis of gold (Au) and silver (Ag) NPs of different sizes has been reported using phenolic compounds extracted from Camellia sinensis [163], which act both as reducing and stabilizing agent. The Ag NPs could be biosynthesized using starch and polyphenols from nopal , Opuntiaficus [167]. The Ag and Au NPs could be synthesized using cereal grains like oat (Avena sativa) and wheat (Triticumaestivum) [168]. Synthesis of Ag and Au NPs using starch as stabilizing agent and β-D glucose as reducing agent has also been reported [169, 170]. Although most of these works report on the biosynthesis of metallic NPs along with the effects of solution pH, aging time, or the nature of bioreductors like glucose, proteins, amino acids, etc., none of them discussed the mechanism of reduction and/or stabilization process. The Copper NPs (Cu NPs) have been attractive for their ability to catalyze chemical reactions [21]. Additionally, Cu possesses a surface plasmon resonance (SPR) which can impart unique optical properties that can be exploited for sensing, imaging, and photonics applications. Unfortunately, one limitation of Cu is that it rapidly oxidizes to form CuO and Cu_2O, and therefore the synthesis of Cu NPs is challenging compared to those of Ag and Au NPs. Oxidation can also result in dramatic shifts of the LSPR, changing or even eradicating its optical response. Most of the syntheses of Cu NPs require the organic solvents, strong reducing agents, polymers, and inert medium. However, there is a need to conduct the synthesis in environmentally benign solvents to get rid of organic pollutants by biodegradable stabilizers. The process needs to be energy

efficient to take care of expensive reactors utilizing inert-gas purging and high temperatures. The green synthesis of Cu NPs has achieved lesser success compared to Ag and Au NPs. Attempts have been made by several groups utilizing plant and leaves extracts as reducing agents as well as stabilizers [171–173]. In all these cases, the formation of Cu NPs has been claimed but detailed structural characterization appears to be lacking. Instead, copper oxide NPs was formed owing to inability of green extracts to reduce Cu atoms from Cu ions. However, they acted as nucleants of copper oxide NPs. Hydrazine hydrate was used as a reducing agent and in presence of NaOH, liberates N_2 gas which created an inert atmosphere in-situ leading to the formation of Cu NPs [79, 173]. In this chapter, synthesis of stable Ag and Au NPs with rice-starch as unique reducing and stabilizing agent will be discussed. Possible mechanisms of reduction and stabilization of the formed Ag and Au NPs have been given. Further, synthesis of Cu NPs and the role of pH on structure and LSPR behavior will be presented as well. The effect of pH on the sol stability and on growth morphology of NPs is investigated. Interaction of the rice-starch with NaOH may lead to change in nature of interaction of stabilizer (rice-starch) which in turn influences the optical properties of sols. The presence of rice-starch as stabilizer influences the growth process of the NPs. Strong adsorption of the polymer would occupy the growth site and reduce the growth rate of the NPs [174].

3.2 Synthesis and Characterization of Ag Nanoparticles

3.2.1 Experimental details

Materials used for the synthesis of Ag NPs included silver nitrate , Sella rice (acquired from local grocery shop), and NaOH. Deionized (DI) water ($\rho > 18.2$ M Ω cm) was used throughout the experiments. The Toshniwal pH-meter was used for measuring pH. For the preparation of rice-starch (RS), 6.0 g rice was boiled at 95 ºC for about 10 min in 100 mL of DI water. After cooling, the mixture was filtered using Whatman filter paper. Two solutions A and B were prepared. Former contains 1.79 g of $AgNO_3$ in 10 mL of water. Latter is made with 0.65g of NaOH in 60 mL of rice gruel. The pH of the rice gruel was kept in the range of 4.5-5.5. Solution B was magnetically stirred for 5 minute by maintaining temperature $\sim$ 60 ºC. Solution A was then added into solution B following protocol reported in earlier investigations [175, 176]. The pH of the sols and various solutions was measured. The light yellow color of solution B changed to brown after addition of 2-3 drops of precursor solution indicating the start of reduction process. After total addition of precursor, the solution turned into a dark brown color. The solution was left for 48 h. The sols, thus obtained, were taken for recording UV-Vis spectra with the help of PERKIN ELMER Lambda XLS+. A drop of sol was dispersed on carbon coated copper grid and dried in ambient conditions. The sample on the grid, thus obtained, was observed under FEI Tecnai G^2 T20 transmission electron microscope operating at 200 kV. Microstructural and structural features were characterized. Identification of the Ag NPs powder was accomplished by by X-ray diffraction (Rigaku, DMAX III with Cu as target).

This result was compared with that of electron diffraction patterns.

3.2.2 Results and discussion

3.2.2.1 LSPR behaviour of Ag NPs sols

The UV-Vis spectra recorded from $AgNO_3$ solution, rice-starch solution after pH adjustment (pH ∼11.0), glucose solution, and Ag sol is displayed in Figure 3.1.

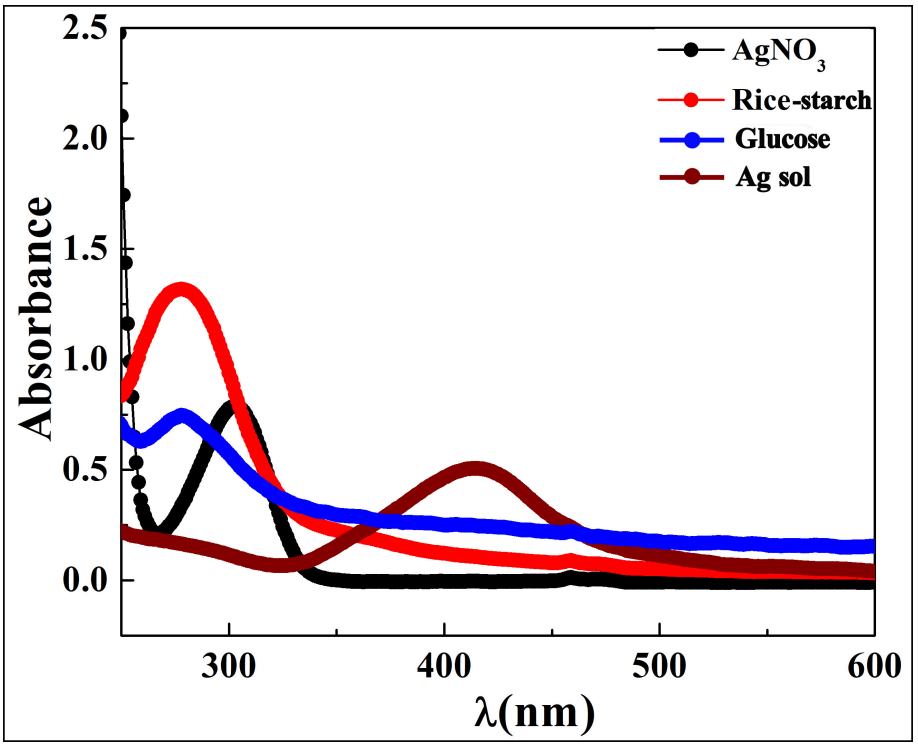

FIGURE 3.1: UV-Vis absorbance spectra of rich-starch stabilized Ag NPs (pH ∼ 11.0) and various solutions used in the synthesis of Ag NPs

The appearance of absorbance peaks at ∼ 270 nm and 300 nm correspond to $AgNO_3$ and glucose solution, respectively. The absorbance peaks of synthetic glucose and rice-starch (pH ∼ 11.0) are observed at ∼ 270 nm suggests *in situ* formation of glucose. Ag NPs suspension exhibits a dark-brown color owing to LSPR, which results

from collective excitation of the free electrons in presence of visible radiations. The LSPR peaks can be used as a tool to predict particle size and stability of the NP suspensions. Figure 3.2 shows the UV-Vis spectra recorded from Ag sols synthesized by varying the pH of the rice-starch solution as 9.0 and 11.0. The nature of spectra with respect to time is depicted to assess stability of the sol under ambient conditions. The absorption peaks range from $\sim$ 400 - 407 nm and $\sim$ 412 - 414 nm for sols with pH 9.0 and 11.0 respectively. UV-Vis results show stability of the sol up to 4 months and 8 months for the Ag NPs stabilized by rice-starch with pH 9.0 and 11.0, respectively. As mentioned above, the wavelength corresponding to absorption peak λ_{max} values changes from 400 nm (t=0) to 407 nm (4 months) indicating a red shift as a result of slight amount of agglomeration (cf. Figure 3.2(c)). Absorbance reduced significantly and it may be attributed to the decreased Ag NPs concentration in the sol with respect to time. The reduced concentration of Ag NPs in the sol could be the result of agglomeration that was seen in the bottom of the test tube. This will be explained further after presenting results of TEM. The sol with pH $\sim$ 11.0 was found to be stable for eight months. The evolution of UV-Vis spectra is shown in the Figure 3.2 (b). There was no significant change in λ_{max} values (from 414 - 412 nm) for the period of eight months (cf. Figure 3.2 (d)). This Ag NPs sol appears to be more stable than that of sol with pH $\sim$ 9.0.

To estimate the size of the NPs in sol state, calculations were performed with software "MiePlotv.3.4" [177]. Several calculations were done by changing the diameter of the particles and compared wavelength of absorption with the experimentally observed UV-Vis spectra. The initial choice of diameter of the NPs as an input in calculation was

made based on TEM investigations. The results of these will be presented in the following section. Further, poly-dispersed spheres in sol with standard deviation of 30% were taken in these computations. It was found that for Ag sol with pH $\sim$ 9.0, best fit between the experimental and theoretical results corresponded to the average particle diameter of 11 nm. This is found in conformity with that of average size measured from TEM micrographs. Both absorbance curves (theoretical and experimental) for Ag sol with pH $\sim$ 9.0 are shown in the Figure 3.3 (a). The best fit of the absorption peak for pH $\sim$ 11.0 Ag sol was obtained for particle diameter of $\sim$16 nm. Figure 3.3 (b) depicts the theoretical

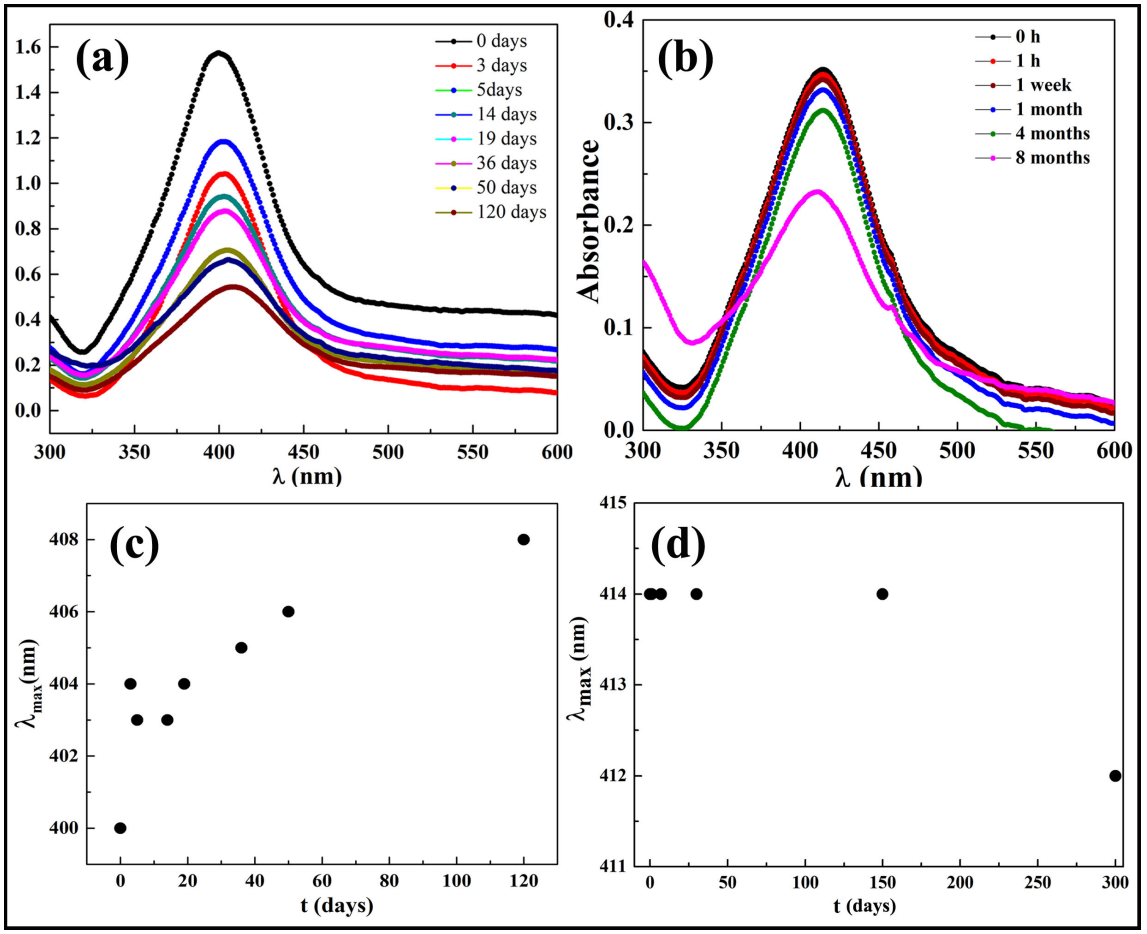

FIGURE 3.2: Temporal evolution of UV-Vis absorbance spectra and LSPR absorbance maxima (λ_{max}) of rice-starch stabilized Ag NPs with pH 9.0 (a, c) and pH 11.0 (b,d) respectively.

and experimental absorbance curves for pH $\sim$ 11.0 sol.

3.2.2.2 Stability Mechanism

The release of glucose by hydrolysis (cf. chapter 1) of starch in basic medium may be retarded. This facilitates the availability of more number of long chain molecules namely amylose and amylopectin in the reaction mixture. As the solution become more basic (pH

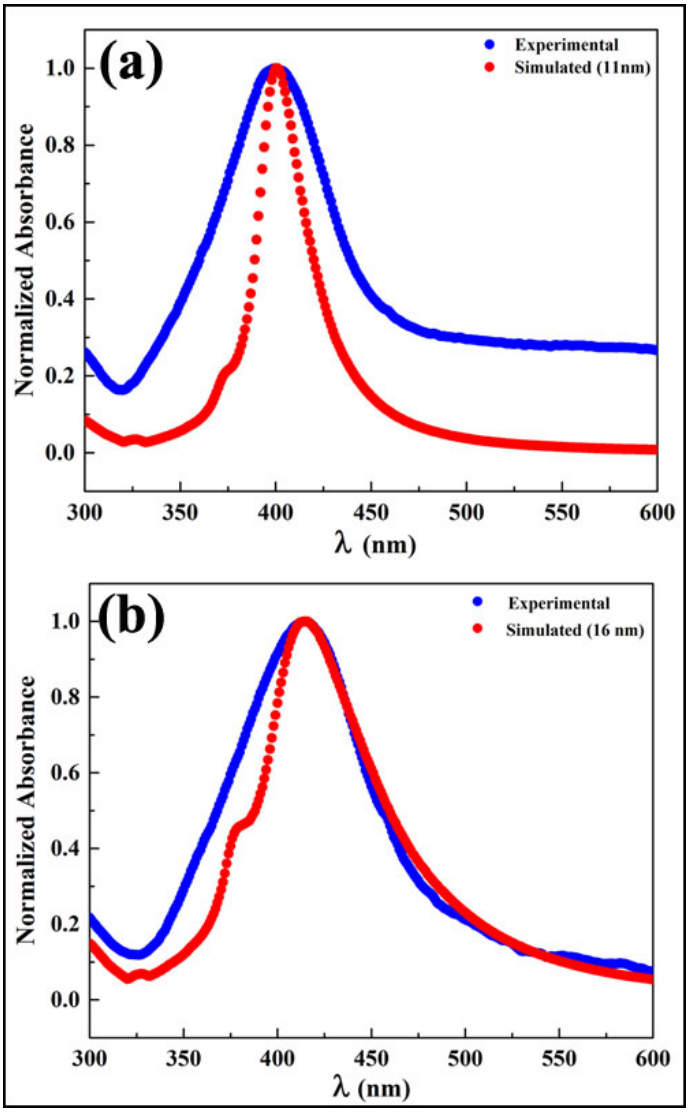

FIGURE 3.3: Comparison of experimental and simulated LSPR curves of Ag NPs with pH 9.0 (a) and pH 11.0 (b), respectively.The choice of size for computation is based on TEM particle size.

$\sim$ 11.0), the presence of these molecules would be more as compared to that of sol with pH $\sim$ 9.0. These long chain molecules can protect the grown Ag NPs from agglomeration. The greater stability of Ag NPs with pH $\sim$ 11.0 (08 months) compared to pH $\sim$ 9.0 sol can be attributed to the presence of more number of long chains in the former.

3.2.2.3 TEM Analysis of Ag NPs sols

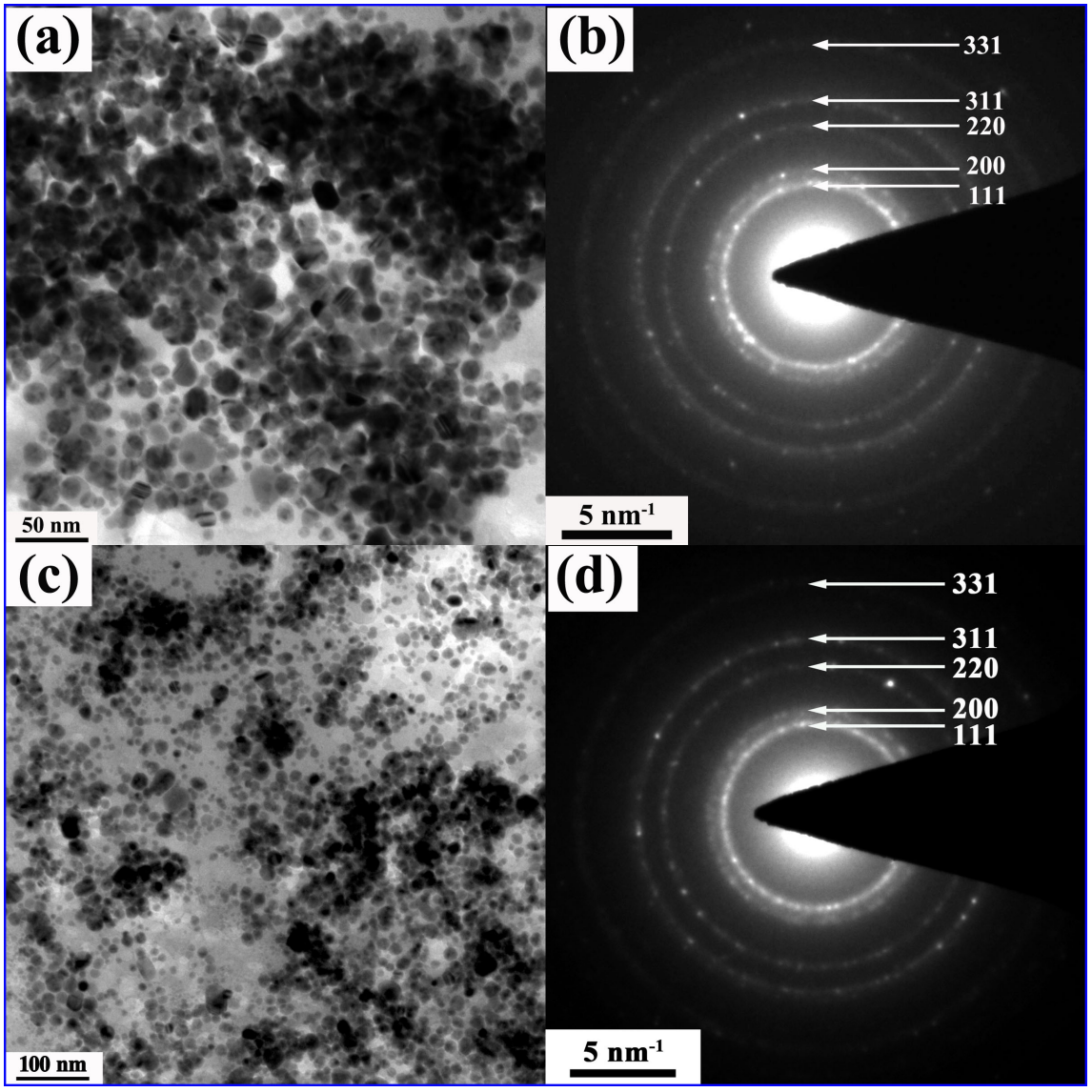

FIGURE 3.4: Representative TEM images (a,c) and corresponding SAD patterns (b,d) of Ag NPs synthesized with pH 9.0 and 11.0, respectively.

The representative bright field TEM image and polycrystalline diffraction pattern (DP) for pH $\sim$ 9.0 Ag NPs sample are shown in Figures 3.4 (a) and (b) respectively. The diffraction rings could be indexed as {111}, {200},{220}, and {311} of FCC-silver having lattice parameter $\sim$ 0.40 nm. The DP shows the presence of sharp spots along with the rings. This may be due to the presence of preferred orientations of some of the particles with sharp faces (shown by arrow marked in Figure 3.4 a). Figures 3.4 (c) and (d) display respectively the representative bright field image and diffraction rings from

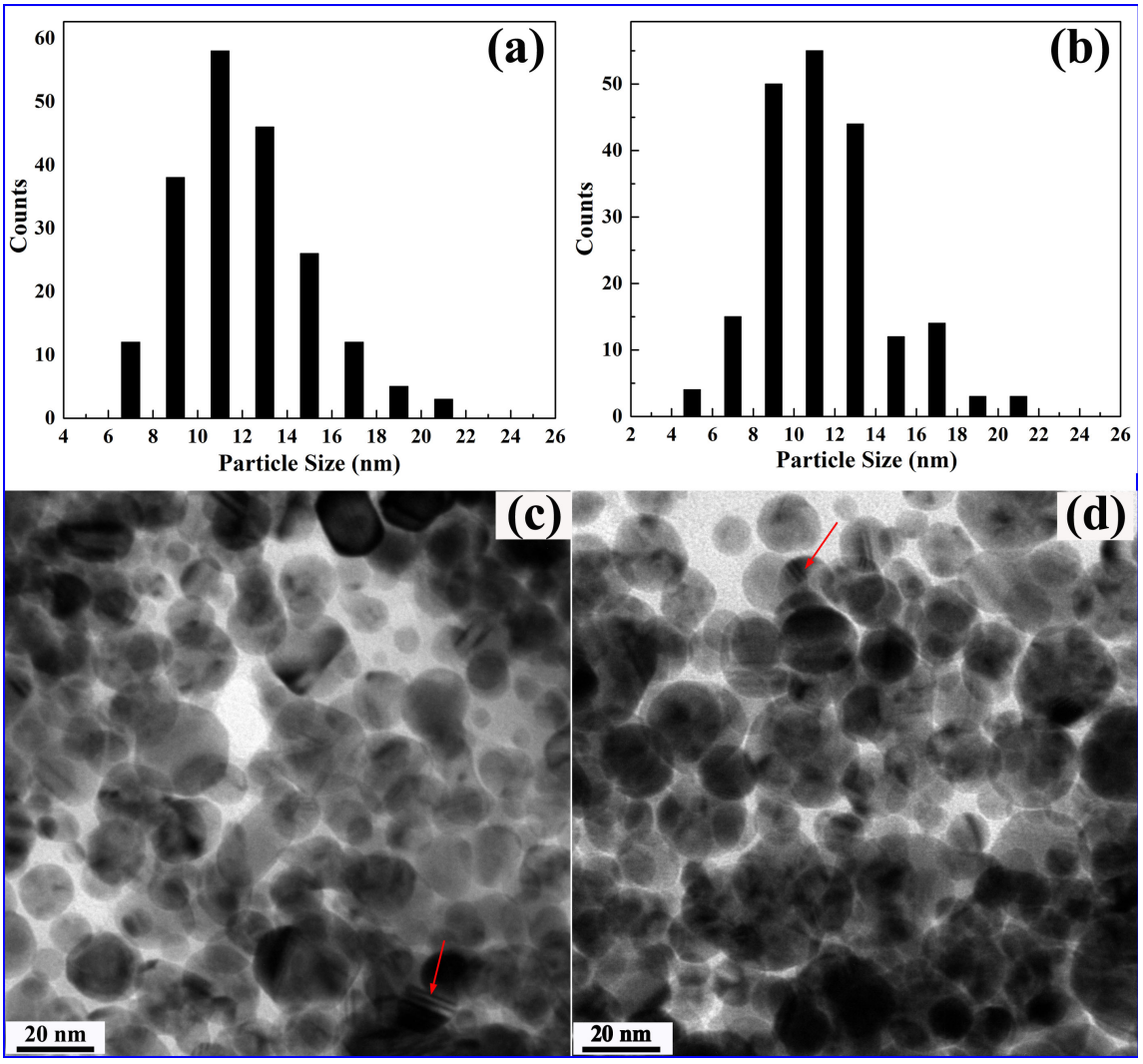

FIGURE 3.5: Particle size histograms (a,b) and high magnification BF TEM images showing growth twins (arrows) in (c,d) of Ag NPs with pH 9.0 and 11.0, respectively.

the Ag NPs with pH $\sim$ 11.0. The rings belong to FCC silver with a lattice parameter of $\sim$ 0.40 nm. Unlike Figure 3.4 (b), one does not see spots around the polycrystalline rings in Figure 3.4 (d) polycrystalline diffraction pattern (DP). This indicates relatively random growth directions of nanocrystalline particles. Thus, uniform shape and size distribution in Ag sample with pH $\sim$ 11.0 is seen. The average particle size of the Ag NPs with pH $\sim$ 9.0 and 11.0 was found to be 11 $\pm$ 3 nm and 12 $\pm$ 3 nm, respectively (TEM images used for the measurements of particle size is given in Appendix A). The size distribution is depicted by histograms in Figures 3.5 (a) and 3.5 (b) respectively. The average size is calculated by measurements of more than 200 particles for both the samples in random fields

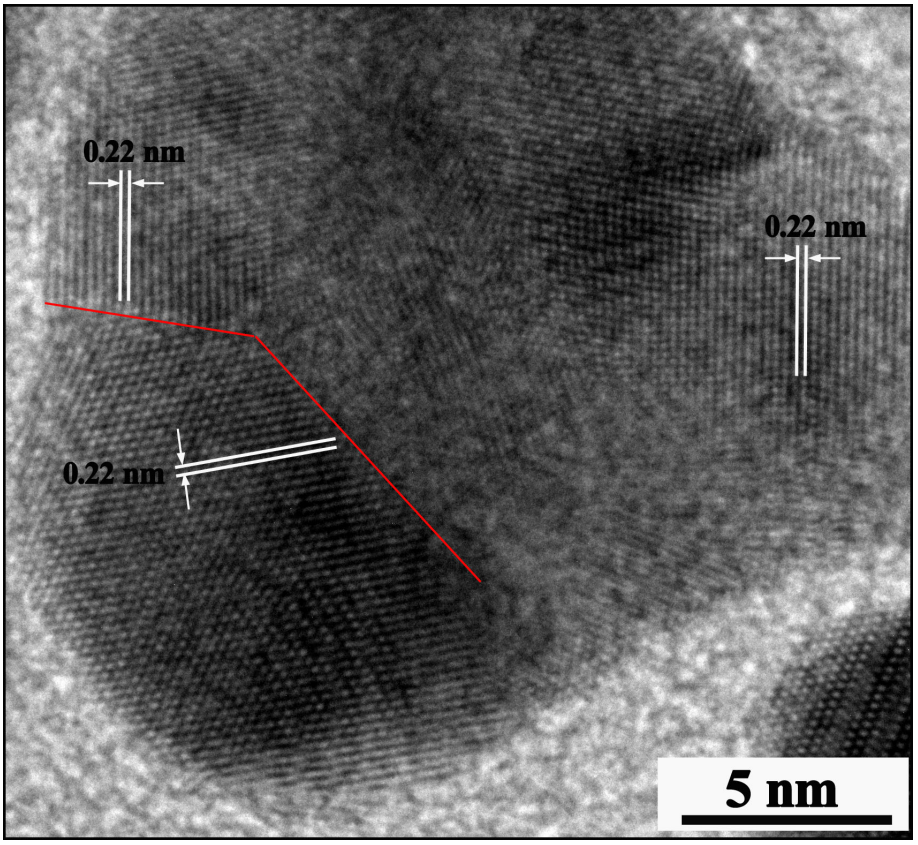

FIGURE 3.6: HRTEM image from a single particle from pH $\sim$ 11.0 sample. The lattice fringe spacing corresponding to d-spacing of $\{111\}$ and grain boundary is depicted.

of TEM view. The high magnification images given in Figures 3.5 (c) and 3.5 (d) clearly bring out the presence of twins in both of them (indicated by arrow). This is consistent with earlier observations of growth twins in nanocrystalline silver. The shape anisotropy in Figure 3.5 (c) is noted for pH 9.0 sample but not in the pH 11.0 one (Figure 3.5 (d)). The representative high resolution TEM image recorded from a particle of sample with pH $\sim$ 11.0 is shown in Figure 3.6. The lattice fringe spacing $\sim$ 0.22 nm corresponding to $\{111\}$ planes of FCC-Ag is depicted in the micrograph. In addition, this particle consists of many grains separated by boundaries as portrayed (by a red line) confirms its polycrystallinity. The XRD patterns of Ag NPs (shown in Figure 3.7) show the peaks corresponding to FCC-Ag. The absence of extra reflections in the patterns confirms that

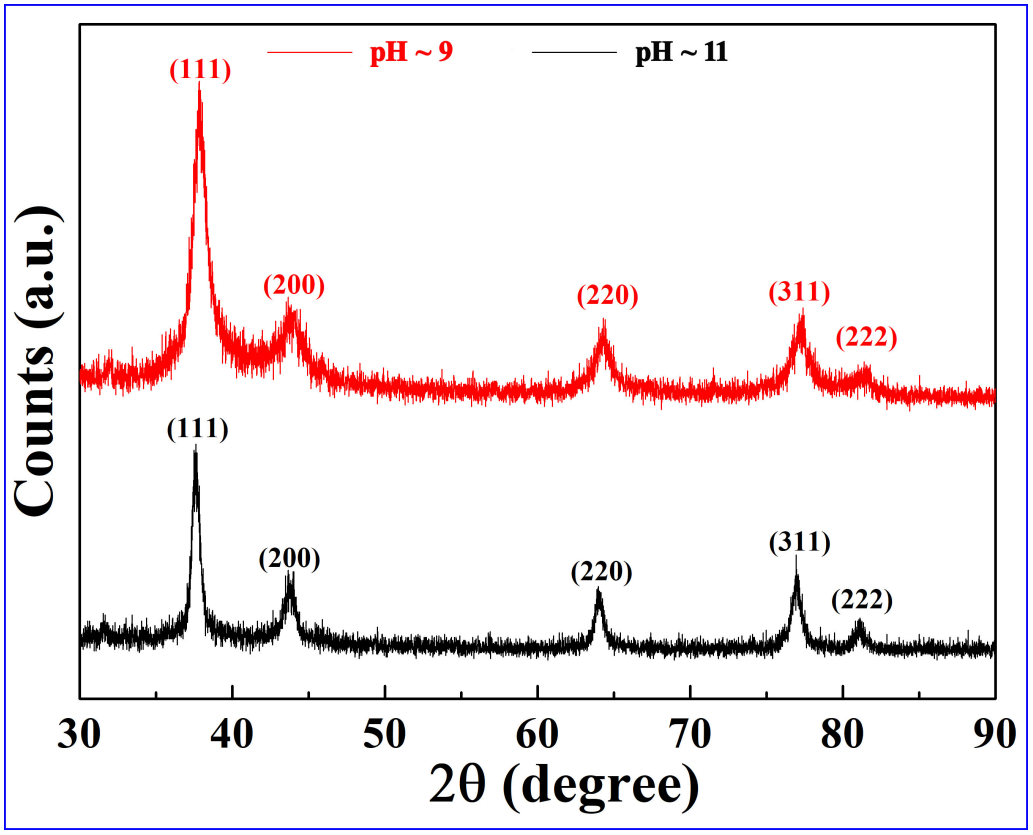

FIGURE 3.7: X-ray diffraction patterns of Ag NPs synthesized with pH 9.0 (red) and 11.0 (black).

the Ag NPs powder is not oxidized.

3.3 Synthesis and Characterization of Au Nanoparticles

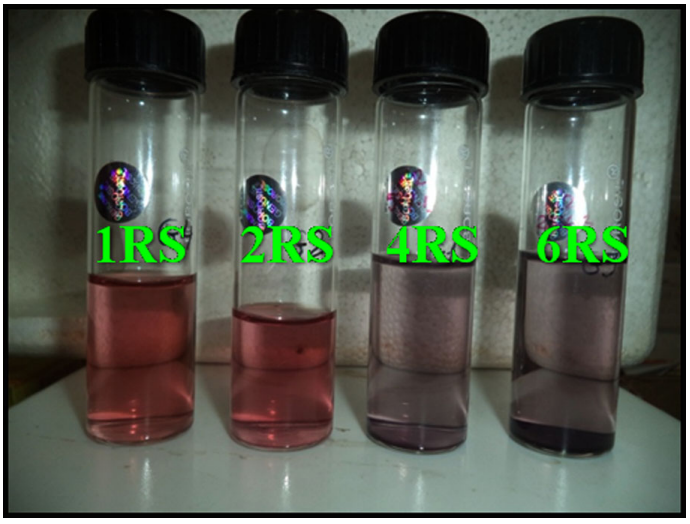

FIGURE 3.8: Rice-starch stabilized Au NPs sols.

3.3.1 Experimental details

3.3.1.1 Preparation of rice-starch extract

The detailed preparation of Sella rice-starch was given in section 3.2.1. In addition to that, rice-starch solution was sterilized using a steel autoclave at 110 ℃ and 69 kPa. To maintain the stability of rice-starch solution, pH was adjusted to $\sim$ 13.0 using NaOH solution. Chloroauric acid ($HAuCl_4$.$3H_2O$) was taken as the metal precursor.

3.3.1.2 Synthesis of Au NPs

Several aqueous solutions with different RS contents were prepared by mixing (20 - x) mL of deionized water and x mL of rice-starch solution (x = 1.0, 2.0, 4.0, and 6.0). Then, 1.0 mL of Au ion solution (5.0 mM) was added to each of the above solutions. After adding Au ions, the solution mixtures were kept in dark avoiding their exposure to any external radiation or stray light. The Au NPs samples are designated according to amount of rice-starch (1 mL, 2 mL, 4 mL and 6 mL) solution as 1RS, 2RS, 4RS, and 6RS, respectively. A spontaneous (1RS and 2RS) and gradual (4RS and 6RS) color change could be noticed after the addition of Au ions in the solutions, indicating the reduction of Au ions.

3.3.1.3 Characterization of Au NPs

Room temperature UV-Vis absorption spectra of the colloidal solutions were recorded at different intervals in a Perkin-Elmer Lambda XLS+ using a square quartz cell of 1.0 cm optical path length. For microscopic observation of the NPs, a FEI Tecnai G^2 T20 transmission electron microscope (TEM) operating at 200 kV was utilized. The samples for TEM observations were prepared by dispersing nanopowders (obtained by centrifugation and cleaning process) in ethanol and a drop on carbon-coated copper grid, followed by drying at room temperature.

3.3.2 Results and discussion

3.3.2.1 Au ions reduction with rice-starch

As discussed in chapter 1, rice constitutes about 76 - 78 % starch, 13 - 14 % moisture, and rest 6 - 8 % proteins, fibers, and fats; wherein, the starch is composed of 20 % amylose and 80 % amylopectin [136]. The amylose consists of lineal chain structure whereas amylopectin possesses branched structure of glucose units. These percentages can vary depending upon rice varieties. During rice-starch preparation, when rice grains were boiled in de-ionized water, the starch grains swell, and both amylose and amylopectin leach out from the granules. At the subjected temperature of boiling ($\sim$ 95 ºC), a very small fraction of both amylose and amylopectin break down into smaller chains of a few glucose units due to the breaking of glycosidic bonds, exposing more aldehyde groups [137–139]. The chain-breaking process continues during sterilization of the solutions (at 110 ºC and 69 kPa), exposing a greater number of aldehyde groups, which act as reducing agent for Au ions. An important parameter to be considered in present synthesis is the pH of the reaction solution, since all the Au NPs were prepared with pH adjustment. The pH of the reaction solutions was measured before pouring gold ions and after dissolving them in the solutions. The pH values of the reaction mixtures were compared before and after the addition of Au ion solution. From the plot presented in Figure 3.9, it was observed that by increasing the concentration of rice-starch (in water), solution basicity increases (e.g. $\mathrm{pH}_{1RS} < \mathrm{pH}_{6RS}$), and by the addition of Au ions, the solutions containing lower contents of rice-starch become less basic (e.g. $\mathrm{pH}_{1RS} < \mathrm{pH}_{6RS}$). The increase in solution pH with increasing rice-starch content is expected as the pH of the used rice-starch solution

was of about thirteen. As the chloroauric acid is highly acidic in nature, by adding gold ions in the reaction mixture, the concentration of protons (H^+) increases, which breaks down some of the glycosidic bonds of amylose and amylopectin (present in the solution) through hydrolysis [140], producing more glucose units and causing a decrease of H^+ ion concentration in the reaction solution. The presence of RS in higher amount in the reaction mixture produces glucose units in higher numbers, causing a lesser decrease of solution basicity.

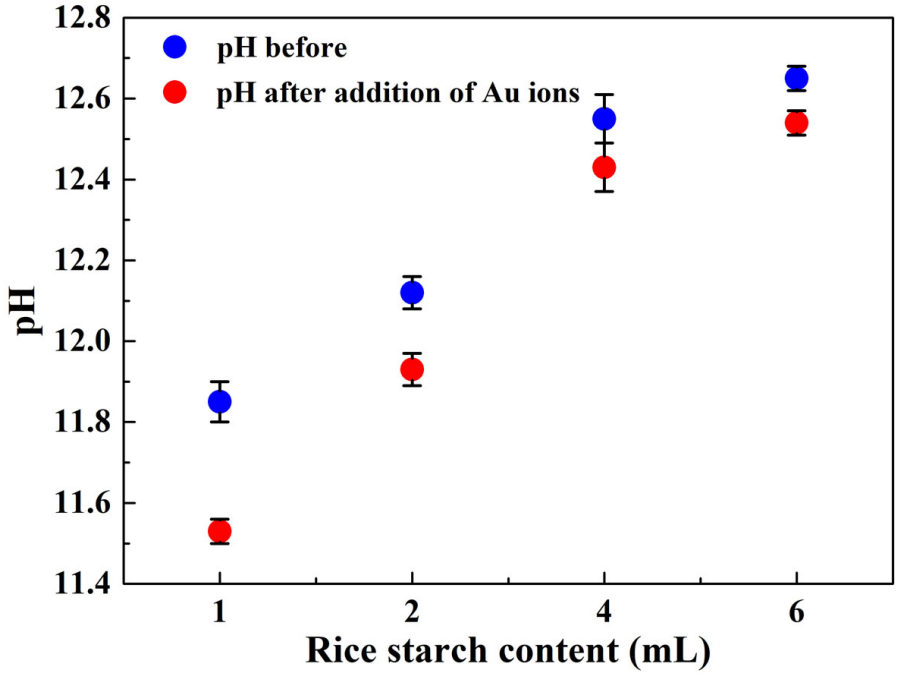

FIGURE 3.9: pH of the reaction mixtures before and after pouring Au ions.

3.3.2.2 Au NPs stabilization with rice-starch

In rice-starch solution *in situ* generation of glucose by hydrolysis of starch facilitates the reduction of Au ions. Besides this excess starch (mostly amylose and amylopectin) present in reaction mixture stabilizes the nucleated Au NPs. As mentioned earlier, the

pH of the reaction mixture varied with rice-starch content, mainly due to the breaking of amylose and amylopectin chains.The amount of amylose and amylopectin chains changes with variation in pH that in turn provides steric stabilization of Au NPs.

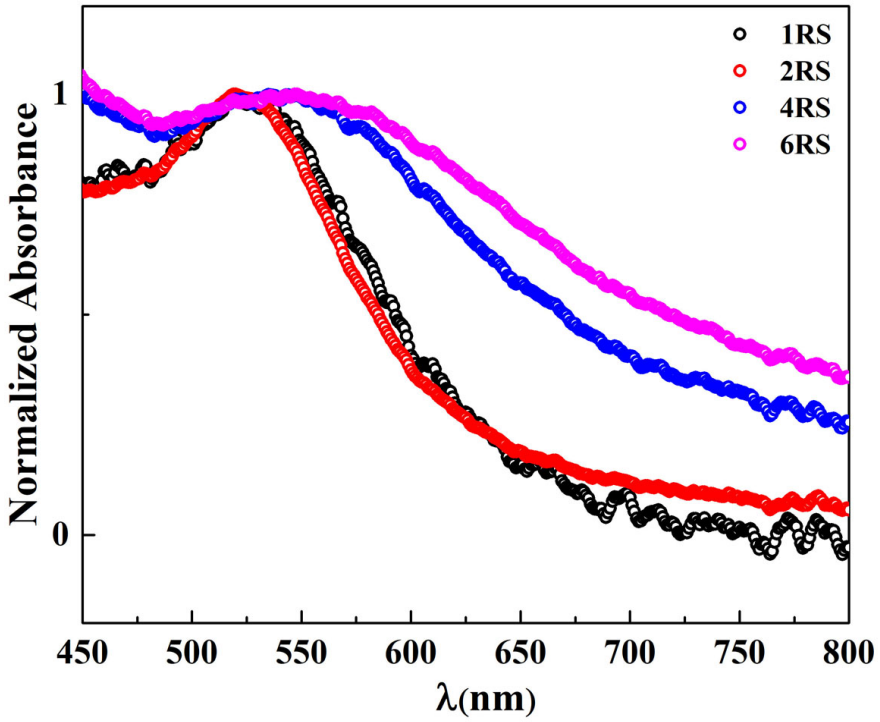

FIGURE 3.10: UV-Vis spectra of 1RS, 2RS, 4RS and 6RS sols after 17 h.

3.3.2.3 LSPR behavior of Au NPs sols

The formation and evolution of Au NPs in the reaction mixtures was studied by UV-Vis absorbance of the reaction solutions at different intervals after the addition of Au ions in them. The absorption spectra of sols recorded after17 h reveal a LSPR peak in between 519 and 548 nm as displayed in Figure 3.10 and are associated to the LSPR of Au NPs [10, 22, 154]. Appearance of LSPR band in the absorption spectra could be noted after about 17 h of preparation of the sols. The LSPR band in all the colloidal samples grows

with time. Initially, the amount of rice-starch in the reaction mixture was appeared to control both the absorbance maxima (λ_{max}) and width of the LSPR band considerably than the reaction time. On increasing the concentration of rice-starch, the LSPR band appeared toward higher wavelengths .This red shift was attributed mainly to an increase of refractive index (n) of the medium by the increase of rice-starch content ($n_{RS} > n_{water}$), as λ_{max} of LSPR band depend on the refractive index of dispersing media [10, 109, 154]. Moreover, the likelihood of red shift of the LSPR band due to the formation of bigger NPs in the reaction solution cannot be ruled out. As can be seen in Figure 3.10, the width of the LSPR band slightly increases by increasing the concentration of rice-starch (w_{1RS}, $_{2RS} < w_{4RS}$, $_{6RS}$), which is associated with the dispersion in size distribution of NPs as supported by their TEM observations (to be discussed in section 3.3.2.4). The nature of

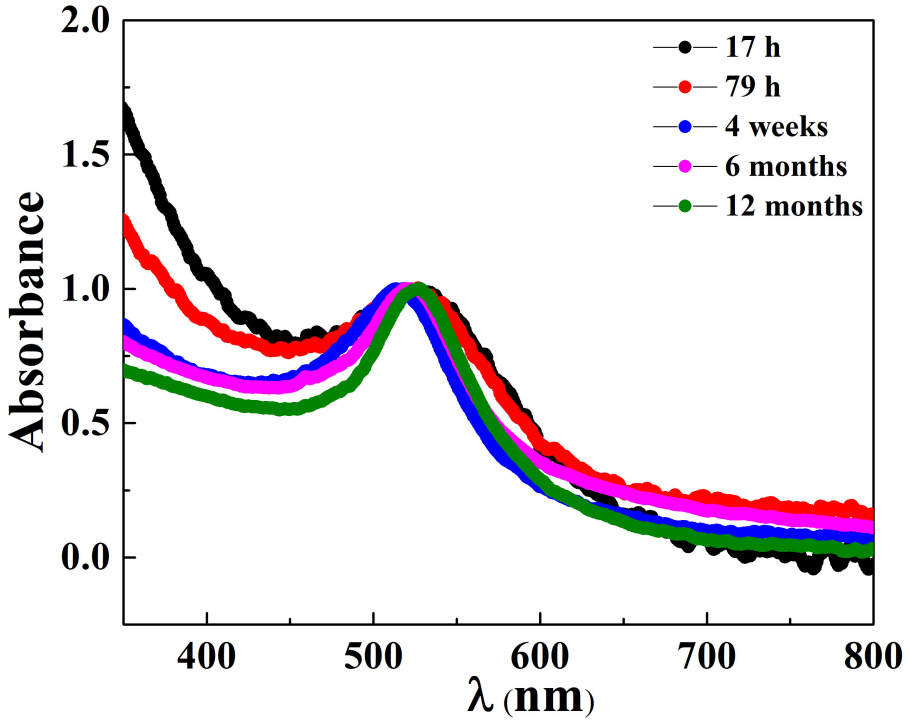

FIGURE 3.11: Temporal evolution of UV-Vis spectra of 1 RS sol from 79 h to 12 months.

UV-Vis spectra of 1RS and 2RS as well as 4RS and 6RS sols was found to be similar. The λ_{max} for the 1RS sol appeared at about 518 nm after 17 h and remains nearly constant up to 6 months, and gradually red shifted to about 528 nm after 12 months as presented in Figure 3.11. This red shift in LSPR peak positions in 1RS (and 2RS) sols could be associated to the aggregation process of Au NPs. For the 4RS (and 6RS) sols, the LSPR peaks observed at $\sim$ 548 nm after 17 h and shifted to $\sim$ 541 nm (blue shift) after 79 h and remain nearly same up to 4 weeks of preparation. A further blue shift ($\lambda_{max} \sim$ 530 nm) with sharper LSPR band was observed after 6 months and no change was recorded thereafter (up to 12 months) (cf Figure 3.12). The variation in LSPR peak profiles with time suggested that initially (17 h and 79 h) concentration of produced Au NPs was less.

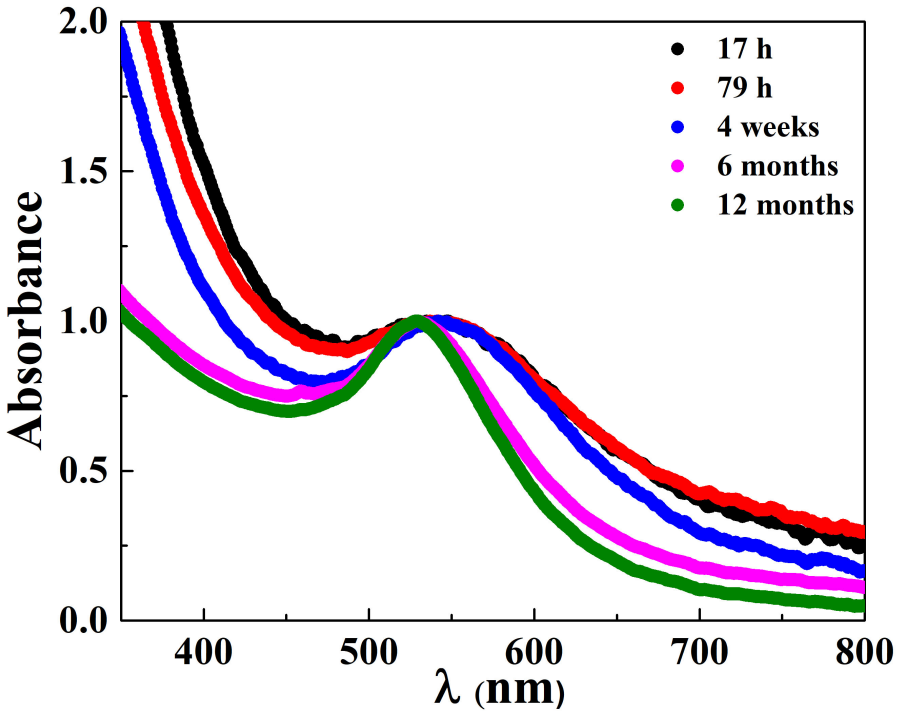

FIGURE 3.12: Temporal evolution of UV-Vis spectra of 4 RS sol from 79 h to 12 months.

This can be inferred from gradual change in color after pouring Au ions, suggested sluggish reaction kinetics. It may be attributed to significant retardation of glucose release owing to basic nature of the reaction mixture containing amylose and amylopectin. The significant blue shift in LSPR peaks with aging for 4RS and 6RS sols may be associated with compositional fluctuation of reaction mixture. The change in composition of reaction mixtures is expected due to continuous reduction of glucose which may initiate secondary nucleation events for unreduced Au ions (present in the solution mixture). A blue shift in LSPR peak for Au sols has been attributed to the size reduction of the NPs [178, 179]. After about 6 months of preparation, the λ_{max} position of the LSPR band stabilized for all the sols and remains nearly same up to 12 months.

3.3.2.4 TEM and HRTEM study of Au NPs

Figure 3.13 shows representative bright field TEM images of the Au NPs formed in each sample and corresponding size distribution histograms are depicted in Figure 3.14 (measured size of at least 300 particles observed in random field of TEM view). A representative SAD pattern of 1 RS sample is depicted in Figure 3.15. The size distribution histogram of 1RS sample shows the formation of well-dispersed Au NPs of sizes in between 11 and 40 nm. A bimodal distribution, with two groups of particles with average sizes of $\sim$ 11 and $\sim$ 25 nm is observed. The particle size distribution histograms for the 2RS, 4RS, and 6RS revealed monomodal size distribution of NPs with average diameters of 26 ± 7, 11 ± 7, and 15 ± 8 nm, respectively (TEM micrographs utilized for particle size measurements are shown in Figures A.2 (d-f) of Appendix A). As can be seen from

their TEM micrographs (cf. Figure 3.10), most of the Au NPs formed in the samples have quasi-spherical morphology while a few with polyhedral shapes, especially for the samples containing lower amount of RS. On the other hand, it seems that the amount of RS in the reaction mixture does not play influential role in the final size of Au NPs, though a small increase in size of the particles is observed for higher RS amount of the reaction mixture. The presence of Debye rings in the DP obtained from 1 RS sample confirms that the particles are crystalline. The DP was indexed and phase was found to be those of FCC-Au with a lattice parameter $\sim$ 0.40 nm, very close to the reported values (ICDD

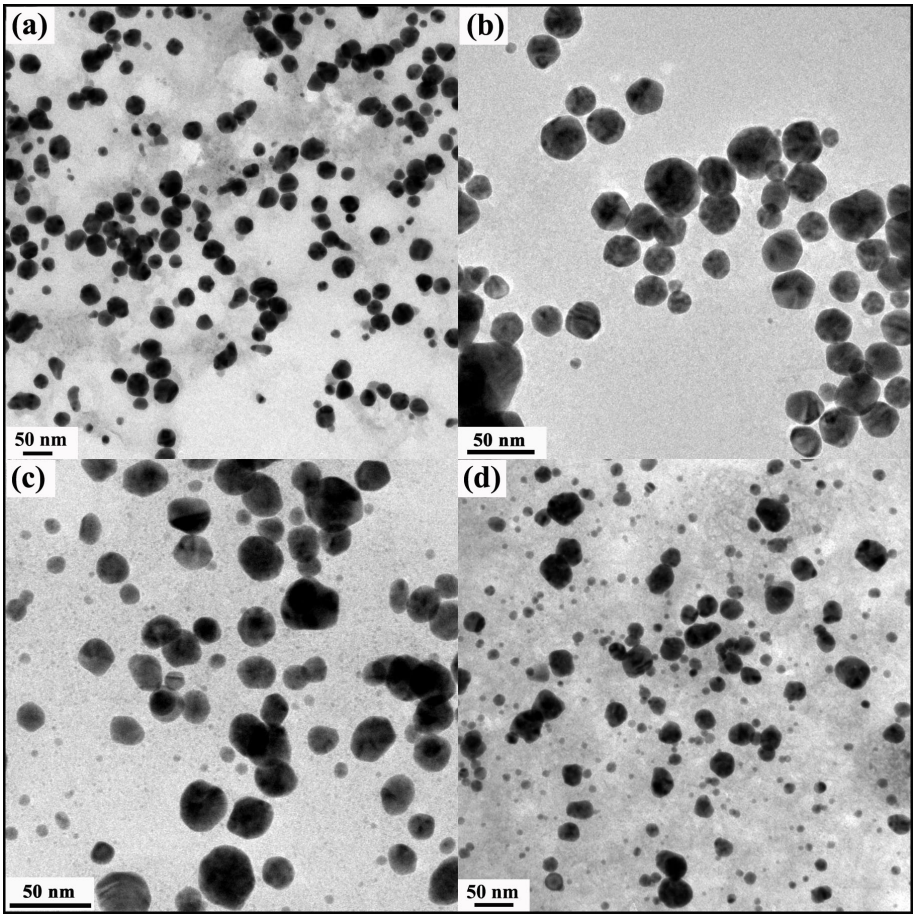

FIGURE 3.13: Representative bright field TEM images of (a) 1RS, (b) 2RS, (c) 4RS and (d) 6RS.

card no. 04-0784). In some cases the integrated intensity values of the peaks are really small or they are so close to another more intense peak that it goes within the error limit of electron diffraction. Keeping this limitation in mind only unambiguous peaks have been reported.

The HRTEM images, representative of each sample are shown in Figure 3.16. As can be seen, all the Au particles are crystalline, frequently with several structural/-growth defects. Figure 3.16 (a) shows a single crystalline faceted Au nanoparticle of

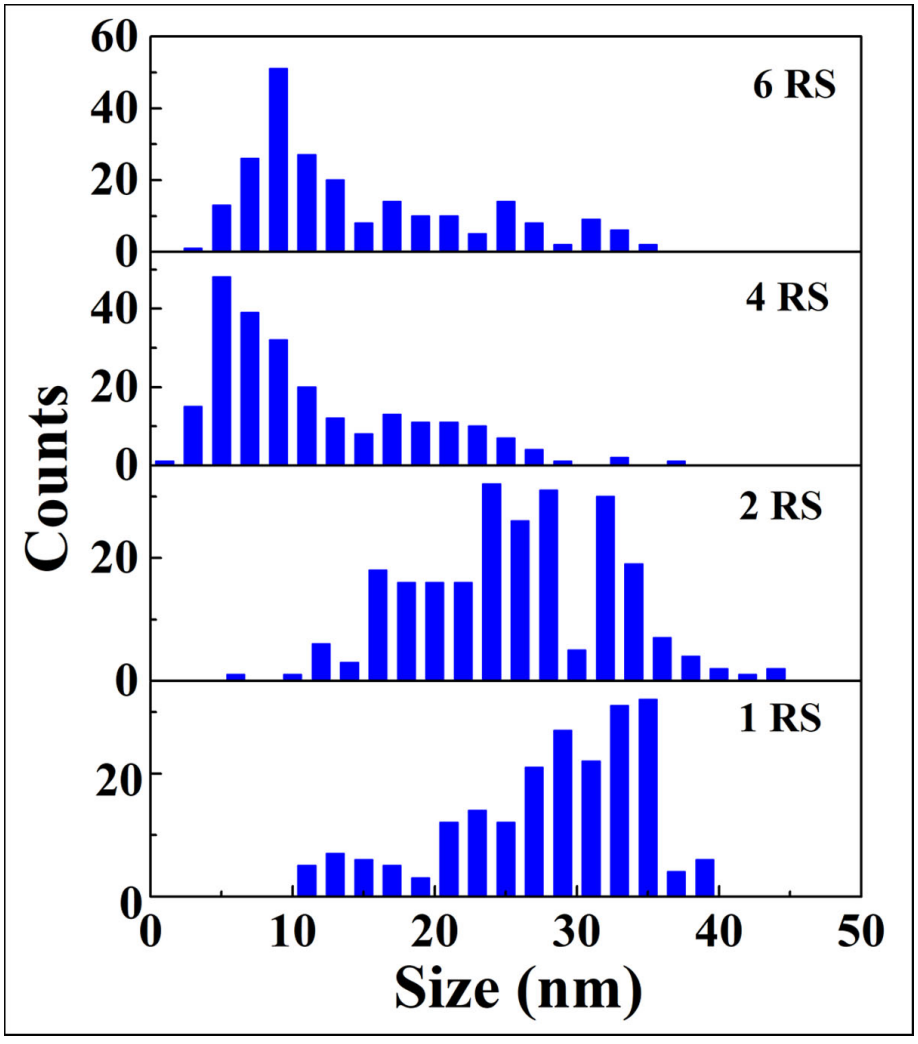

FIGURE 3.14: Size distribution histograms of 1RS, 2RS, 4RS and 6RS.

size $\sim$ 16 nm typical to the 1 RS sample. An analysis of the facets reveals that $\{111\}$, $\{001\}$, and $\{112\}$ surface facets being exposed by the nanoparticle. Moreover, the preferred atomic attachment along $< 111 >$ directions is observed. Figure 3.16 (b) displays a polycrystalline Au NP of size $\sim$20 nm from 2 RS sample, revealing lattice spacing of $\sim$ 0.22 nm and corresponds to $\{111\}$ planes of FCC-Au in different grains. The representative HRTEM micrograph of 4 RS sample shown in Figure 3.16 (c), displaying two grains separated by defects. The lattice spacing of $\sim$ 0.22 and $\sim$ 0.19 nm corresponding to $\{111\}$ and $\{200\}$ planes of FCC-Au is observed in two different regions of the particles. Figure 3.16 (d) shows HRTEM image of a single crystalline nanorod with length $\sim$ 22 nm of 6RS sample displaying lattice fringes correspond to $\{111\}$ planes. In addition, lattice fringes of spacing corresponding to $\{111\}$ plane in a NP is also depicted as inset in

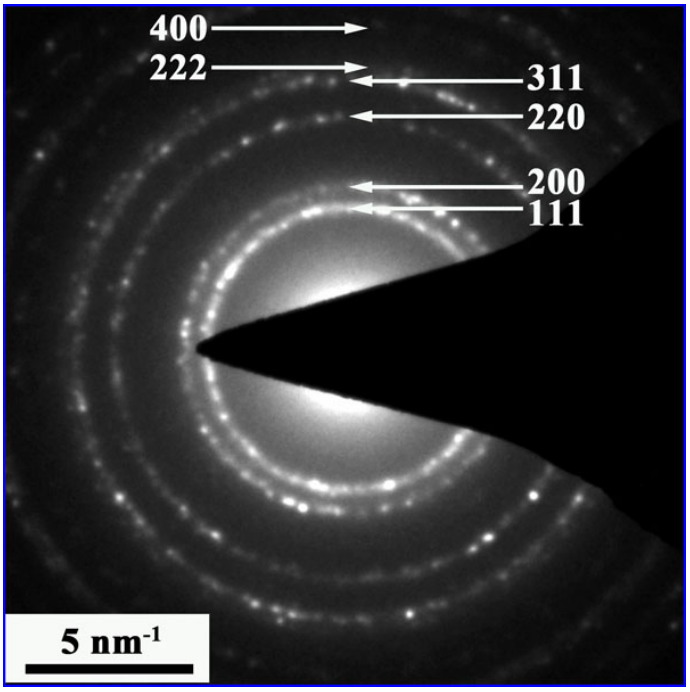

FIGURE 3.15: Representative SAD pattern from 1RS sample.

Figure 3.16 (d). From the analysis of HRTEM images of the synthesized Au NPs, crystalline grains with exposed faces such as {111}, {200}, and {112} of FCC-Au lattice have been observed. In general, samples 1RS, 2RS, and 6RS produced polyhedral shapes with well defined facets. On the other hand, sample prepared with the amount 4RS appears to produce smaller nanocrystals as well as quasi spherical NPs.

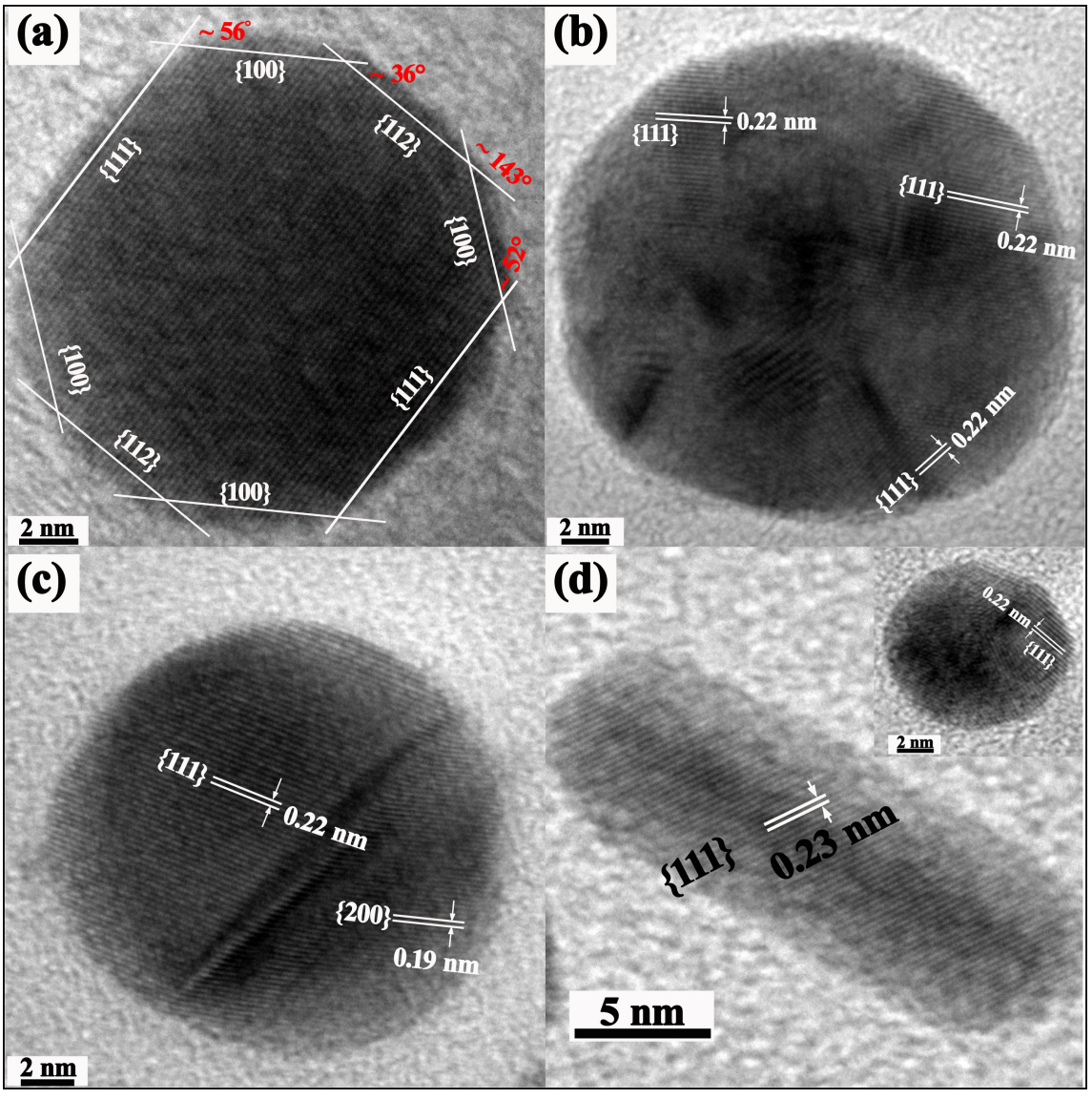

FIGURE 3.16: HRTEM images of (a) 1RS, (b) 2RS, 4RS(c) and 6RS with a polyhedral particle as inset (d).

3.4 Synthesis and Characterization of Cu Nanoparticles

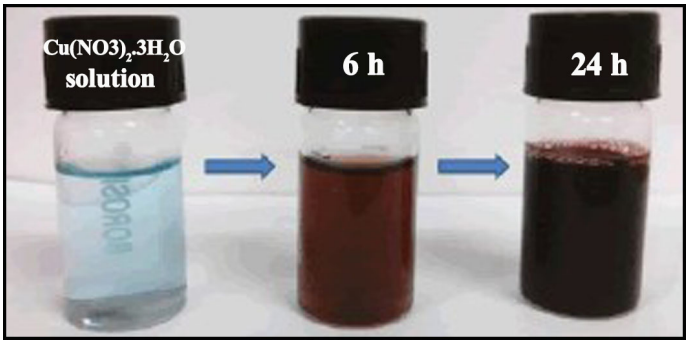

FIGURE 3.17: Rice-starch stabilized Cu NPs sol.

3.4.1 Experimental details

The synthesis protocol requires 20 mL rice-starch (in gruel form). The detailed preparation method of rice-starch has been given in the section 3.2.1. The pH of this solution was kept at $\sim$ 8.0, 10.0, and 11.0, respectively, by adding appropriate amount of NaOH solution. They are referred to as S1, S2 and S3 from here onwards. Twenty mL (0.01M) Cu $(NO_3)_2.3H_2O$ aqueous solution was mixed in each of them. In these solutions, 20 mL (1M) of hydrazine hydrate (HH) was added drop-wise. Various colours (henna, orange, light brown, and dark brown) were observed during the process of addition of HH. The resulting Cu NPs suspension was stirred for about ½ h for the completion of reaction. This suspension was kept for 24 h in ambient condition. The dark-brown colour changes to red-brown. The Cu sols and powder obtained after centrifugation was characterized by UV-Vis spectrometer, TEM and XRD. The stability of the sols has been assessed through monitoring λ_{max} of the LSPR absorbance spectra.

3.4.2 Results and discussion

3.4.2.1 LSPR behavior of Cu NPs

Figure 3.18 a shows the UV-Vis absorbance spectra of S1, S2, and S3 sols. The LSPR peaks λ_{max} corresponding to the sols S1, S2, and S3 were observed at $\sim$ 584 nm, 589 nm, and 595 nm, respectively, and increases with pH. The LSPR peak width of the sol S1 is $\sim$ 64.0 nm which is more than those of S2 and S3 sols. This suggests that the particles in the sol S1 has more polydispersity. The UV-Vis spectra of the sample S3 is plotted as a function of time is shown in Figure 3.18 b. The λ_{max} at $\sim$ 584 nm was observed from S3 for 2 days, 2 weeks and 4-week time. This shows that shelf life of sol S3 is about 1 month. The stability can be attributed to the presence of dense layer of large polysaccharide molecules from rice-starch as discussed in earlier sections.

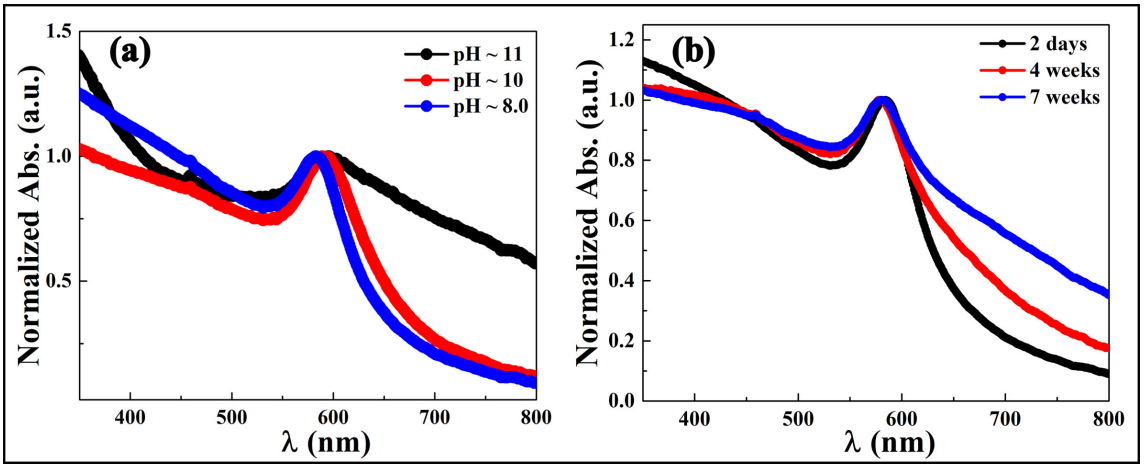

FIGURE 3.18: (a) UV-Vis absorbance spectra of S1,S2 and S3 sols and (b) temporal evolution of UV-Vis spectra of sol S3.

TABLE 3.1: Characteristics of Cu NPs in sol as well as in powder form.

Sample designation	**pH**	**Coherently scattered domain size (nm)**	**LSPR absorbance maxima (λ_{max})**
S1	8.0	21	584
S2	10.0	22	589
S3	11.0	21	595

3.4.2.2 X-ray diffraction study

Table 3.1 gives designation of the samples studied in terms of pH and coherently scattered domain size. Figure 3.19 shows the XRD patterns of S1, S2, and S3, respectively. In all samples, diffraction peaks corresponding to (111), (200) and (220) FCC copper were observed. Coherently scattered domain sizes (Table 3.1) are calculated with the help of full width at half maximum (FWHM) using Scherrer formula after making necessary corrections for instrumental broadening. In samples (S1, S2 and S3), no significant change in the coherently scattered domain size with respect to pH was found. In all the samples, cupric nitrate peaks are also observed (cf. Figure 3.19). However, the yield of FCC-Cu was observed to be higher with increasing pH and is maximum for the sample S3. The Presence of copper oxide was not found in any of the samples. Although, all the Cu precursor was not reduced and yet no sign of oxidation of Cu NPs was observed. Therefore, sample S3 is being investigated for growth morphology and structure by TEM.

3.4.2.3 TEM investigation of Cu NPs

The bright field TEM image, corresponding SAD pattern, size distribution histogram, and high resolution TEM micrograph of a particles is depicted in Figure 3.20. The particles are mostly spherical with average size $\sim$ 11 nm have been observed (TEM micrographs

utilized for particle size measurements are shown in Figures A.2 (a-c) of Appendix A). The rings corresponding to {111}, {220}, {222}, etc. could be indexed to those of FCC-Cu. HRTEM image from a particle depicts fringe spacing $\sim$ 0.20 nm corresponding {111} plane of FCC-Cu. The average size of the Cu NPs (S3) measured from the TEM micrographs is less than that of coherently scattered domain size of the Cu NPs. This can be associated with the sampling in two different characterization techniques. In TEM, one takes a dilute suspension of the sample and drop cast it on the TEM grid. It is highly likely that the particles with bigger size could not be placed on the grid. On the other hand, in XRD experiment such restrictions are not there. The Cu NPs (S3) synthesized

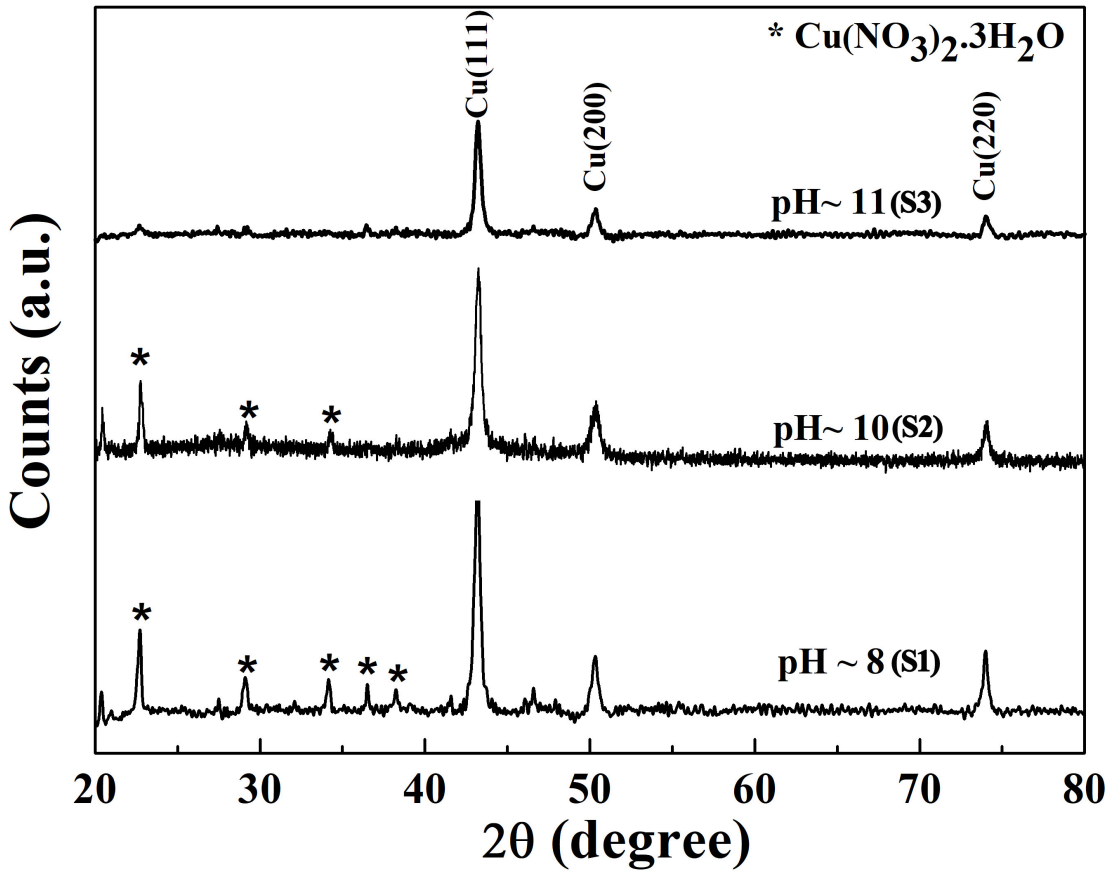

FIGURE 3.19: XRD patterns of Cu NPs with varying pH (S1,S2 and S3).

with the experimental condition will be used for the synthesis of Ag-Cu and Au-Cu alloy NPs. This aspect will be discussed in the next chapter.

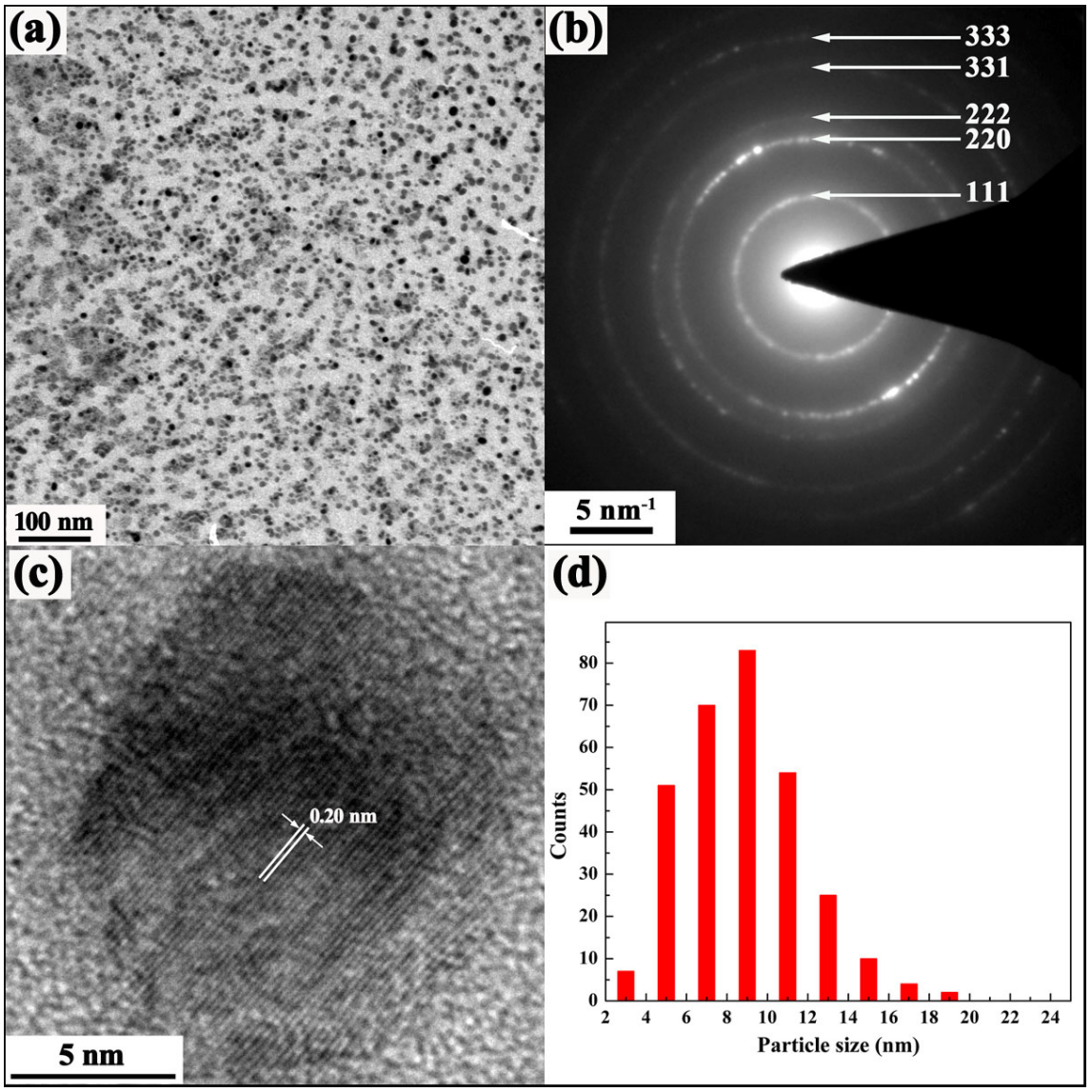

FIGURE 3.20: (a) TEM image, (b) corresponding SAD pattern, (c) HRTEM image from a particle and (d) size distribution histogram of Cu NPs synthesized keeping pH $\sim$ 11.0.

3.5 Conclusions

A geen method has been developed successfully to synthesize NPs of Ag, Au, and Cu where rice-starch served as unique reducing agent and stabilizer. The release of glucose *in situ* during the hydrolysis of rice in presence of NaOH acted as reducing agent for synthesis of Ag and Au NPs. The presence of amylose and amylopectin in adequate amount owing to basic nature of the reaction mixture helped to contain the growth of Ag and Au NPs. For Cu NPs, rice-starch could serve as stabilizer only owing to its inability to reduce Cu^{2+} to Cu^{0}. The stabilities of Ag, Au, and Cu sols are observed more than $\sim$ 12 ,$\sim$ 24 and $\sim$ 1 months, respectively. The yield of the Cu NPs is found to be pH dependent and maximum for pH $\sim$ 11.0 in this synthesis protocol.